

See discussions, stats, and author profiles for this publication at: <https://www.researchgate.net/publication/263396210>

Role of Subcolloidal (Nanosized) Precursor Species in the Early Stage of the Crystallization of Zeolites in Heterogeneous Systems

ARTICLE *in* LANGMUIR · JUNE 2014

Impact Factor: 4.46 · DOI: 10.1021/la5012296 · Source: PubMed

CITATION

1

READS

72

10 AUTHORS, INCLUDING:



Nan Ren

Fudan University

40 PUBLICATIONS 1,123 CITATIONS

[SEE PROFILE](#)



Maja Dutour Sikirić

Ruđer Bošković Institute

43 PUBLICATIONS 374 CITATIONS

[SEE PROFILE](#)



Tea Mišić Radić

Ruđer Bošković Institute

20 PUBLICATIONS 162 CITATIONS

[SEE PROFILE](#)



Vesna Svetlicic

Ruđer Bošković Institute

83 PUBLICATIONS 868 CITATIONS

[SEE PROFILE](#)

Role of Subcolloidal (Nanosized) Precursor Species in the Early Stage of the Crystallization of Zeolites in Heterogeneous Systems

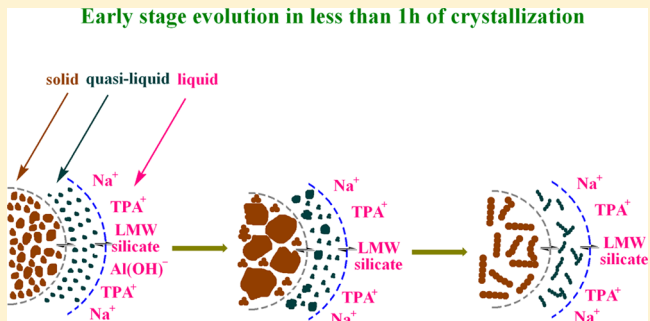
Nan Ren,^{*†} Sanja Bosnar,[‡] Josip Bronić,[‡] Maja Dutour Sikirić,[§] Tea Mišić,^{||} Vesna Svetličić,^{||} Jian-Jiang Mao,[†] Tatjana Antonić Jelić,[‡] Mirko Hadžija,[⊥] and Boris Subotić^{*‡}

[†]Department of Chemistry, Shanghai Key Laboratory of Molecular Catalysis and Innovative Materials, Institute of Catalysis, and Laboratory of Advanced Material, Fudan University, 220 Han Dan Road, Shanghai 200433, P.R. China

[‡]Division of Materials Chemistry, Laboratory for the Synthesis of New Materials, [§]Division of Physical Chemistry, Laboratory for Synthesis and Processes of Self-Assembling of Organic Molecules, ^{||}Division for Marine and Environmental Research, Laboratory for BioElectrochemistry and Surface Imaging, and [⊥]Division of Molecular Medicine, Laboratory for Molecular Endocrinology and Transplantation, Ruđer Bošković Institute, Bijenička 54, 10000 Zagreb, Croatia

S Supporting Information

ABSTRACT: A critical analysis was carried out for the purpose of understanding the role of subcolloidal (nanosized) (alumino)silicate precursor species in the early stage of crystallization of zeolites in heterogeneous systems (hydrogels). The formation and evolution of these subcolloidal species in both the solid and the liquid phases were investigated by various experimental methods such as scanning electron microscopy (SEM, FE-SEM), transmission electron microscopy, atomic force microscopy, particle size analysis, pH measurement, atomic absorption spectroscopy, and dynamic light scattering, after careful separation of intermediates from reaction mixture by two-step centrifugation treatment. The results revealed that a chain of processes (i) the formation of low-molecular-weight (LMW) silicate species, by dissolution of Al-enriched amorphous silica, and their aggregation into about 3 nm sized primary precursor species (PPSs), (ii) the formation of larger (~3 to ~15 nm sized) silicate precursor species (LSPSs) by a rapid aggregation/coalescence of PPSs, (iii) the formation of “gel” (primary amorphous precursor) by a random aggregation of LSPSs at room temperature, and (iv) the formation of the worm-like particles (secondary amorphous precursor) occurred in the solid phase during heating of the reaction mixture (hydrogel) from room temperature to 170 °C. It is interesting that almost the same processes occur in the liquid phase but with decreased rate according to the relative low concentration of LMW silicate species. With the above described findings, it is highly expected that the manipulation of crystallization pathway through controlling the formation/evolution of precursor species in the initial stage of the process can be achieved.



1. INTRODUCTION

Zeolites are crystalline silica or silica-alumina materials with periodic 3-D framework and well-defined microporous structure. Because of their properties such as acidity, porosity, and molecule-sieving effect, zeolites have been widely used as catalysts, adsorbents, ion exchangers, and microreactors in petroleum refining and fine chemical industry.¹

Because the performances of zeolites, relevant for their applications, are largely determined by their structural, particulate, and morphological properties and even chemical compositions,² the perfect, controllable synthesis of zeolite with tailored properties, to meet the criteria of diverse applications, becomes one of the most important tasks in the research domain. The above aim can only be realized with the thorough understanding of critical processes (nucleation, crystal growth) occurring during crystallization.

In general, there are two basic synthesis methodologies for zeolites: crystallization from heterogeneous systems (alumi-

nosilicate hydrogels) and crystallization from homogeneous systems (initially clear aluminosilicate solutions).^{2,3} The essential difference between these two approaches is the presence (former case) or absence (latter case) of the amorphous solid phase (gel) during the initial stage of crystallization.^{2,3}

On the basis of numerous studies of the mechanisms of crystallization of silicalite-1 in homogeneous systems,^{4–16} it was concluded that the critical step of the crystallization process is the formation of the subcolloidal (Na,TPA)-silicate (TPA = tetrapropylammonium) particles, which are precursor species for nucleation and crystal growth of MFI-type zeolites.⁹

For such systems, Schoeman⁴ and later on de Moor et al.⁵ assumed that primary precursor species (PPSs) for zeolite

Received: April 7, 2014

Revised: June 19, 2014

Published: June 24, 2014

crystallization are predominantly amorphous, 2–4 nm sized silica particles with trapped TPA⁺ ions. Kirschhock et al.⁶ have argued that PPSs are preformed nanometer-sized ($1.3 \times 4.0 \times 4.0$ nm) slabs (“nanoslabs”) of silicalite-1. Fedeyko et al.⁷ and Provis et al.⁸ suggested that PPSs are ~3 nm sized ellipsoidal particles bearing a core-shell structure with silica at the core and the TAA (tetraalkylammonium) cations at the shell.

The evolution of PPSs during heating of the reaction mixture (initially clear solution) is also interpreted in different ways, while Schoeman⁴ and later on Fedeyko et al.⁷ and Provis et al.⁸ suggested that the evolution of nanoparticles during heating can be described by Ostwald ripening mechanism, de Moor et al.⁵ and Davis et al.¹⁵ proposed a mechanism of direct aggregation of PPSs to form zeolite crystals. Finally, Kirschhock et al.⁶ suggested that “nanoslabs” combine together to form “nanoblocks”, which then further combine with each other to generate extended MFI framework. Besides the cases in MFI-type zeolites, the *in situ* methods have also been applied for the study of crystallization mechanisms of zeolites with other kinds of framework topologies.^{17,18}

However, the commercial MFI and other types of zeolites are usually synthesized in heterogeneous systems.^{19–21} Hence, the studies of the processes occurring during crystallization of zeolites in heterogeneous systems are important not only from the scientific viewpoint but also for the precise control of the product properties to meet the demands of specific applications and reducing the production cost. Although it is reasonable to assume that some of the occurrences/processes observed in homogeneous systems are also identical to the crystallization of zeolites in heterogeneous systems,^{22–25} the methods applied for studying the critical processes occurring in homogeneous systems cannot be used for studying the critical processes occurring in heterogeneous systems because of the appearance of an abundant amount of amorphous phase in the initial stage, the crystallization at high temperature (>150°C), and the presence of considerable amount of aluminum species.

These are possible reasons that there are only few studies in which the knowledge accumulated during investigation of the crystallization of MFI-type zeolites in homogeneous systems has been applied and, to some extent, modified for the analysis and explanation of the processes occurring during crystallization of MFI-type zeolites in heterogeneous systems.^{22–25}

In our recent work, the crystallization processes from a dilute but still heterogeneous, unstirred system (having the composition of $12.5\text{Na}_2\text{O}-\text{Al}_2\text{O}_3-60\text{SiO}_2-8\text{TPABr}-4000\text{H}_2\text{O}$) was carefully studied using a series of methods to characterize the changes of particulate properties in both the solid and the liquid phases.²⁴ Although the general feature of crystallization pathway in the sequence, primary aluminosilicate amorphous precursor (gel, formed during room-temperature aging of the reaction mixture) → secondary amorphous aluminosilicate precursor (“worm-like” particles (WLPs)) → tertiary aluminosilicate amorphous precursor (condensed aggregates (CAs)) → final crystalline end products (ZSM-5) in the form of polycrystalline aggregates (only the amorphous phase of CAs can be finally transformed into crystalline one), has been revealed to a large extent, the microstructure of the solid phase in the initial stage of crystallization and the relevant processes that occurred in the liquid phase of the system have not yet been considered satisfactorily. Thus, taking into consideration that the knowledge on the processes, occurring at molecular or submicrometer level, in the reaction mixture during early stage crystallization process is extremely important

for the further course of crystallization and possible control of the tendency of processes to generate materials with new structural types and properties, the objective of this work is focused on the investigation of the formation of nanosized precursor particles in both the solid and the liquid phases of hydrogels and their evolution during early stages of crystallization of zeolites in heterogeneous systems through a critical analysis. The previously mentioned reaction mixture, typical for the synthesis of MFI-type zeolites, is used again as the model system.²⁴

2. EXPERIMENTAL SECTION

2.1. Materials. The reagents used for the preparation of the investigated reaction mixtures (hydrogels) were: sodium hydroxide (NaOH, analytical grade, Kemika, Croatia), sodium aluminate (NaAlO₂, 54 wt % Al₂O₃, 41 wt % Na₂O, Riedl de Haen), fumed silica (SiO₂, surface area 175–225 m²/g, Alfa Aesar), tetrapropylammonium bromide (TPABr, analytical grade, Alfa Aesar), and deionized water. All chemicals were used as received without any purification.

2.2. Preparation of the Reaction Mixture and Its Further Treatments. The appropriate volume of the solution was prepared by mixing freshly prepared sodium hydroxide solution (30 wt %), sodium aluminate, and TPABr in deionized water to form a transparent solution. For example, the detailed procedure was carried out by dissolving 2.55 g of NaOH in 5.95 g of H₂O; after the sodium hydroxide was completely dissolved, 0.53 g of NaAlO₂ was added to the solution, followed by the addition of 5.9 g of TPABr; then, 194.05 g of water was added to the mixture. When the homogeneous, transparent solution was obtained, such solution was heated to the desired temperature ($T_H = 20, 35, 50, 65$, and 80 °C); then, 10 g of fumed silica is added to the thermostated solution, under vigorous stirring. Such prepared reaction mixtures ($12.5\text{Na}_2\text{O}-\text{Al}_2\text{O}_3-60\text{SiO}_2-8\text{TPABr}-4000\text{H}_2\text{O}$) were “aged” at the preparation temperatures for $t_A = 1$ h without stirring; then, the solid and liquid phases were separated by centrifuging. A part of the reaction mixture (RM), prepared at 20 °C (room temperature; *rt*) was divided into two autoclaves. The autoclaves containing the reaction mixture were put into an oven preheated at crystallization temperature ($T_H = T_c = 170$ °C). The moment when the autoclaves containing the reaction mixture were put into the preheated oven was recorded as the zero time ($t_c = 0$) of the crystallization process. At predetermined crystallization times ($t_c = 1$ and 4 h), the selected autoclaves were taken out from the oven and cooled to the ambient temperature. After cooling the autoclave, the reaction mixture was centrifuged to separate the solid from the liquid phase.

2.3. Solid–Liquid Separation. Heating of RMs under static conditions establishes a concentration gradient, from which the precursor species, generated/developed during the heating, are distributed among the solid and the liquid phase. Among other factors (temperature and time of heating), the distribution is mainly determined by the size and density of the participating precursor species. Thus, the two-step centrifugation, first at lower speed, to separate solid phase in aggregated form, followed by centrifugation at higher speed, to separate discrete colloidal species dispersed in liquid phase, has been used for the preparation of the solid and liquid samples for analyses/characterizations. For this, each of the reaction mixtures, prepared and treated as described in Section 2.2, was at first centrifuged at lower speed (lower speed centrifugation (LSC); 12 000 rpm, with a relative centrifugal force of 17 000g) for 20 min. The clear liquid phase (supernatant) above the sediment was carefully removed without disturbing the solid phase (sediment). The solid phase was redispersed in deionized water and centrifuged repeatedly. The procedure was repeated until the pH of the liquid phase above the sediment was ~9. The washed solid phase was dried at 80 °C for 10 h, and then cooled to room temperature and stored in desiccators over silica gel. A part of the liquid phase was used for determination of Si or Al concentrations in the liquid phase, pH of the liquid phase, and DLS (dynamic light scattering) analysis of the particles present in the liquid

phase. Another part of the liquid phase was further centrifuged at higher speed (higher speed centrifugation (HSC); 60 000 rpm, with a relative centrifugal force of 225 000g) for 60 min. The clear liquid phase (supernatant) above the sediment was carefully removed without disturbing the solid phase and used for determination of Si or Al concentrations in the liquid phase, pH of the liquid phase, and DLS analysis on the particles present in the liquid phase. The solid phase, separated by HSC, was redispersed in deionized water and centrifuged repeatedly. The procedure was repeated until the pH of the liquid phase above the sediment was ~9. Such prepared solid phases were characterized by transmission electron microscopy (TEM).

2.4. Characterization. Concentrations of aluminum and silicon in the solutions, separated by either LSC or LSC/HSC from the RMs heated at different temperatures, were determined by atomic absorption spectroscopy (AAS, AAnalyst 200, PerkinElmer).

The pH of the solutions, separated by either LSC or LSC/HSC from the RMs heated at different temperatures, was measured using a Corning Pinnacle 555 pH/ion meter. The pH meter was calibrated with pH 9.0 and 12.0 buffer solutions at 25 °C. The accuracy of the pH meter was ± 0.01 pH units.

The size distribution curves of the particles present in the solutions, separated by either LSC or LSC/HSC from the RMs heated at different temperatures, were measured by DLS approach using Zetasizer Nano-ZS (Malvern) equipped with green laser (523 nm). Intensity of scattered light was detected at the angle of 173°. For each sample, 10 measurements were performed. The data processing was done by the Zetasizer software 6.20 (Malvern Instruments). The size distributions are reported as volume and number distributions. The size distribution curves of the solid samples, separated by LSC from the RMs heated at different temperatures, were determined with a Malvern Mastersizer 2000 laser light-scattering (LLS) particle size analyzer.

Scanning electron microscopy (SEM) measurements of the solid samples were performed by either a Philips XL30 D6716 or FEI Nova NanoSEM for field-emission model.

TEM experiments were carried out with a JEOL JEM-2010 instrument at operating voltage of 200 kV.

Atomic force microscopy (AFM) of the solid samples was performed by multimode scanning probe microscope with Nanoscope IIIa controller (Veeco Instruments) with a vertical engagement (JV) 125 μm scanner. Sharp silicon cantilever probes (TESP, Veeco) with nominal spring constant of 42 N/m and nominal frequency of 320 kHz were used. The powdered solid samples were suspended in ultrapure water (1 g/dm³) and stirred for 1 h and sonicated for 30 min. Suspension was diluted by ultrapure water so that the final suspension contained 10 mg of powder/dm³. Five microliters of the final suspension was pipetted directly onto freshly cleaved mica. Following deposition, the mica sheets were placed in enclosed Petri dishes for several hours at a relative humidity of 50% to evaporate the excess water. All images were collected using tapping (semicontact) mode because it is well-adapted to soft samples due to the nearly complete reduction of lateral forces.

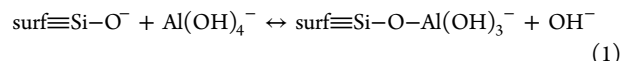
3. RESULTS AND DISCUSSION

In the dilute heterogeneous crystallization system, the general feature of the crystallization process can be described by a chain of “transformations”: “gel” → WLPs → CAs → crystalline end product in the form of polycrystalline aggregates.²⁴ However, the detailed changes occurring during the first stage of crystallization pathway, that is, the formation of “gel” and its “transformation” into WLPs have not been studied in our previous work. Now, on the basis of obtained results, the relevant processes can be explained as follows:

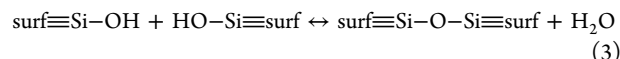
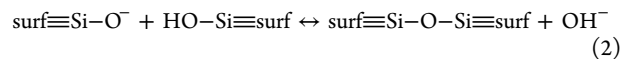
During mixing the reactants at room temperature (*rt*), the fumed amorphous silica, used as silica source, is dispersed in water solution of sodium hydroxide (0.3472 mol dm⁻³ = 12.72 g NaOH per 1 kg of RM), sodium aluminate (0.0278 mol dm⁻³ = 3.002 g NaAl(OH)₄ per 1 kg of RM), and tetrapropyl

ammonium bromide (0.111 mol dm⁻³ = 27.098 g TPABr per 1 kg of RM). The starting pH of the liquid phase (pH 13.22) is determined by the concentration of the OH⁻ ions that arise from both the added sodium hydroxide and sodium aluminate.

Reaction of the OH⁻ ions from solution with the surfaces of the particles of amorphous silica (Scheme 1A) causes the formation of surface $\equiv\text{Si}-\text{OH}$ and $\equiv\text{Si}-\text{O}^-$ groups²⁶ (Scheme 1B). At the same time, in accordance with the principle that “in the solution containing a mixture of silicate species, aluminum preferentially complexed with larger silicate species, almost immediately,”²⁷ the Al(OH)₄⁻ ions from solution react with deprotonated silanol groups on the silica surfaces and form surface Si—O—Al bonds (eq 1).²⁸



This step causes the formation of amorphous silica enriched with aluminum^{20,24,25,29} (Scheme 1C1,C2) and therefore the decrease in the concentration, $C_{\text{Al}}(L)$, of aluminum in the liquid phase during short-time *rt* aging of RM. (See SI-1 in the Supporting Information.) Coagulation of the negative charged particles of the fumed amorphous silica by the actions of Na⁺ and TPA⁺ ions²⁸ causes the precipitation of the amorphous silica (Scheme 1D1; see also Figure S1 in the Supporting Information). The collisions of the silica particles during coagulation/precipitation enable the condensation reactions of the surface $\equiv\text{Si}-\text{OH}$ and $\equiv\text{Si}-\text{O}^-$ groups of the colliding particles of amorphous silica (eqs 2 and 3).²⁶ Thus, the $\equiv\text{Si}-\text{O}-\text{Si}\equiv$ bridges between the neighboring particles of the precipitated amorphous silica (Scheme 1D2) can be formed, that is



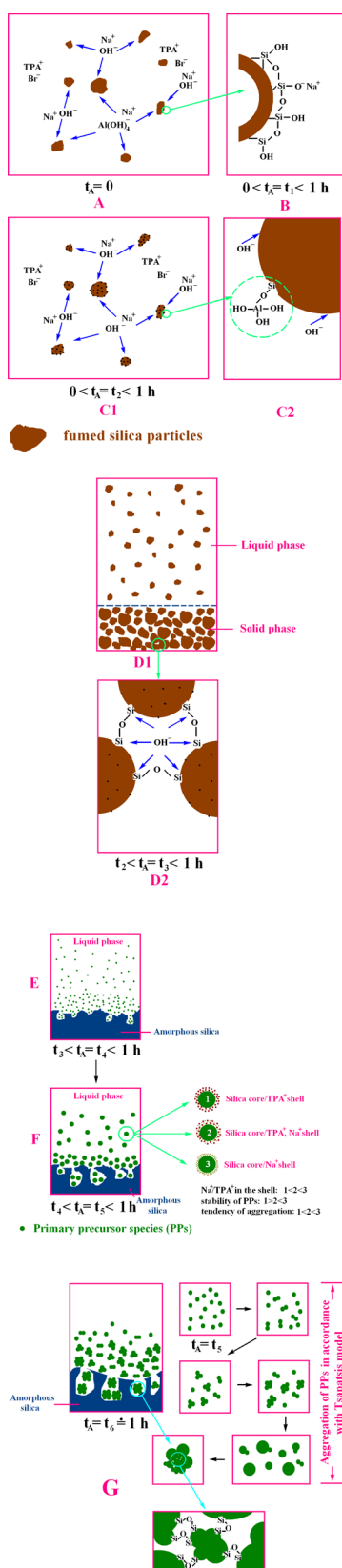
The previous processes result in a rapid formation of larger aggregates (1.3–400 μm ; Figure 1A,B) composed of the particles of amorphous silica (bordered by yellow circle in Figure 1C), having the size in the hundreds of nanometers range, and rickety aggregates of discrete particles having the size in the 100 nm range (bordered by red circle in Figure 1C).

Dissolution of Al-enriched amorphous silica, during *rt* aging of RM, produces low-molecular-weight (LMW) silicate species (monomers, dimers, oligomers).^{30–35} The concentration of the LMW silicate species is the largest at the place of their formation (surface of the amorphous silica) and decreases toward the bulk of the liquid phase (Scheme 1E).²⁴

Now, taking into the consideration that small ~ 3 nm-sized subcolloidal particles (PPSs) can be formed in alkaline silicate solutions at even room temperature,^{4,5,7,36,37} it is reasonable to assume that in the investigated RM, the formation of PPSs is most possible at/near the surfaces of the dissolving amorphous silica and that this possibility decreases toward the bulk of the liquid phase (Scheme 1F).

Because the solid phase contains only ~ 5 wt % of TPA,²⁴ the formation of the “de Moor-type”⁵ PPSs cannot be expected for at least two reasons: (i) The content of TPA in the inorganic–organic composite species (IOCSs),^{5,22} by which the “de Moor”-type PPSs can form, is about the same as the content of TPA in well-crystallized MFI-type zeolites. Thus, the PPSs should contain more than 10 wt % of TPA, which is about two times larger than the content of the TPA in the current solid

Scheme 1. Schematic Presentation of the Processes Occurring during Room-Temperature Aging of RMs



phase of RM. (ii) The TPA⁺ ions in the solid phase of RM were revealed as only in the state of physical adsorption, as shown in our previous investigation,²⁴ which is in contradiction with the

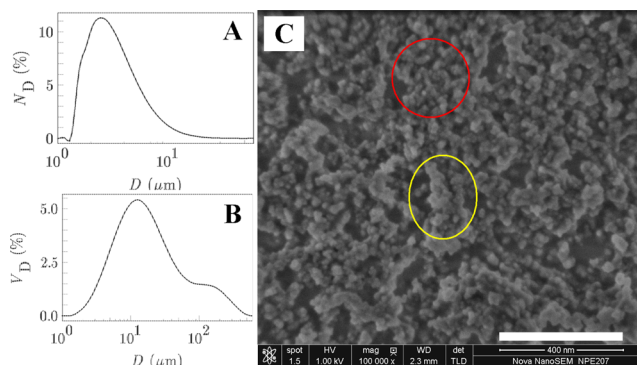


Figure 1. PSDs by number (A) and by volume (B) and FE-SEM image (C) of the solid phase of the RM aged at *rt* for 1 h. N_D is number percentage and V_D is volume (mass) percentage of the particles having the spherical equivalent diameter D . Scale bar in panel E represents 400 nm.

strong interaction of TPA⁺ ions with siliceous species in the “de Moor”-type PPSs.^{5,22} In addition, identification of the PPSs as “nanoslabs” is not reliable because the solid phase of RM is XRD, IR, and ED amorphous,²⁴ while the nanoslabs exhibit the structural feature characteristic for well-crystallized MFIs.⁶ Thus, it is reasonable to assume that the PPSs generated in heterogeneous systems are the most probable core(amorphous silica)-shell(TPA⁺,Na⁺) features formed by a stepwise aggregation/condensation of monomeric silicate species, as was, for the formation of PPSs in homogeneous systems, suggested by Lobo and coworkers (Scheme 1F).^{7,8,36,37} Although authors postulated that the formation of stable nanoparticles at room temperature appears to be in equilibrium and that only at higher temperatures (70–90 °C) do nanoparticles grow reversibly through an Ostwald ripening mechanism,³⁶ the presented results show that the nanoparticles of different sizes (~3 to ~15 nm or more; see Figure 2 and Figures S4 and S5 in the Supporting Information) are present in the solid phase of the investigated RM even after short (1 h) aging at room temperature (Scheme 1G). This indicates that most of the formed PPSs are “unstable” and immediately aggregate into the larger precursor species (Scheme 1G) through collision/coalescence processes.^{15,38–41} This “instability” of the core-shell PPSs is probably caused by the presence of Na⁺ ions in the investigated RM: Namely, because in the investigated RM the PPSs are formed in a mixed (TPA⁺, Na⁺) cationic environment, it is reasonable to assume that the nanoparticle shell can be composed of either TPA⁺ ions or Na⁺ ions or by mixtures of TPA⁺ and Na⁺ ions in different proportions (Scheme 1F). As in the investigated RM, the concentration of Na⁺ ions is more than three times higher than the concentration of TPA⁺ ions, and it is reasonable to assume that the PPSs with the Na⁺ shell predominate; the small amount of TPA (only ~5 wt %)²⁴ in the solid phase corroborates this assumption. This is, at the same time, a possible reason that despite the declared stability of the silica(core)–TPA(shell) PPSs^{7,15,36,37} they are able to agglomerate into larger (> 3 nm) precursor species³⁷ (Scheme 1G).

On the basis of the well-known fact that the collision efficiency increases with the increasing difference in the size of colliding particles^{15,40,41} and that the collision frequency decreases with the increase in the overall size, $D_{\Sigma} = D_n + D_m$ of the colliding particles,⁴¹ it is reasonable to conclude that the addition of PPSs on the already formed aggregates is the

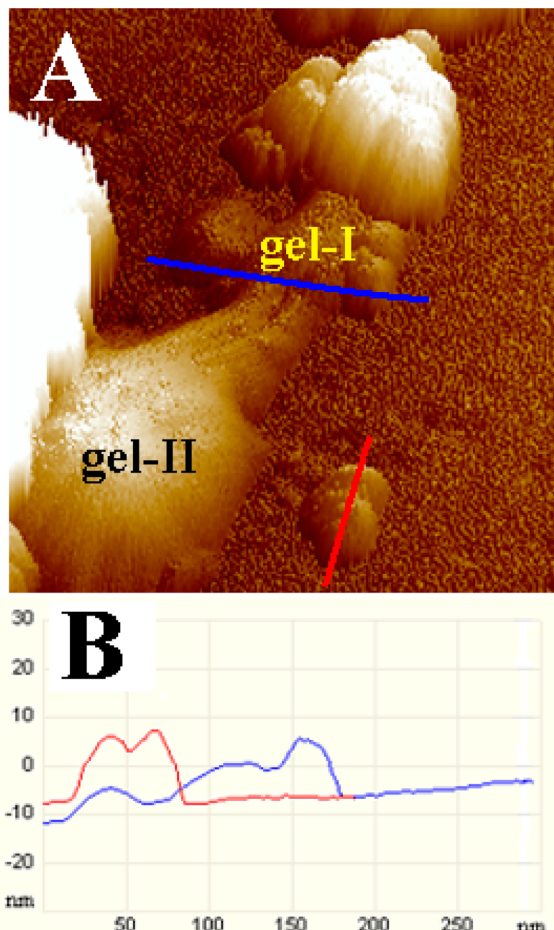


Figure 2. (A) AFM image of the solid phase of the RM aged at rt for 1 h. (B) Section analysis of the AFM image in panel A.

dominant process of the formation of the precursor nanoparticles having $D > 3$ nm (Scheme 1G). Of course, the mutual collisions of the already formed aggregates are, in the smaller extent, also possible. This finally results in the formation of discrete precursor nanoparticles of different sizes: larger silicate precursor species (LSPSs) (Scheme 1G). The formation and existence of the near spherical discrete precursor particles having the size in the range from 3–15 nm (Figure 2) leads to the postulation that the rate of particles collisions is lower than the rate of coalescence of the colliding particles.^{15,39,40}

In this way, the formation of the precursor species of different sizes, during a short-time, room-temperature aging of the RM, is the most consistent with the mechanism of the formation of the particles B_n , proposed by Davis et al.¹⁵ A limitation in the size (<20 nm; see Figure 2, Figures S4 and S5 in the Supporting Information) of the discrete precursor species is probably caused by the decrease in the “coalescing potential” with the increase in the particles size: Namely, the rate of coalescence decreases with the decreasing surface energy and thus with the overall size, D_{Σ} , of the colliding particles.³⁸ This is, at the same time, the reason that the “gel” formed during short-time, room-temperature aging of the RM is composed of both discrete (“gel”-I) and partially or fully coalesced precursor species (“gel”-II) of different sizes (Scheme 1G) in the range from 3 to <20 nm (Figure 2). This is consistent with the finding that agglomeration is the dominant

process when the rate of collision is higher than the rate of coalescence.^{39,40}

Because of the inertness of the surface Si–O–Al bonds (negative charged Al-centers—black dots in Scheme 1C1,D2),⁴² the dissolution of aluminosilicate species does not occur during the *rt* aging of RM. Even because the protective action of the Al-centers is not limited on the first coordination sphere only but also on the several neighboring coordination spheres,⁴² it can be reasonably assumed that the dissolution causes the formation of pores in the particles of amorphous silica (Scheme 1E,F) and further enrichment of the undissolved silica with aluminum. This process is, to a large extent, consistent with the formation of mesopores in aluminosilicate materials during their desilication in alkaline media.^{42–45} Hence, the LSPSs, formed during the short-time (1 h) *rt* aging of the RM, are predominantly siliceous species.

The solid phase formed during the short-time (1 h) *rt* aging is XRD, IR, and ED amorphous, as was revealed by our previous investigation.²⁴

Concentration of the LMW silicate species in the liquid phase of the RM, aged at *rt* for 1 h (see SI-1 in the Supporting Information), is insufficient for the formation of the PPSs and their further aggregation into LSPSs. This is the reason that the liquid phase contains only the ionic species: hydrated TPA⁺ ions, aluminate ions, and LMW silicate anions and of course Na⁺, OH⁻, and Br⁻ ions.

Heating of RM causes intensive morphological changes of the solid phase of the RM (Figures 3 and 4 and Figures S6–S13

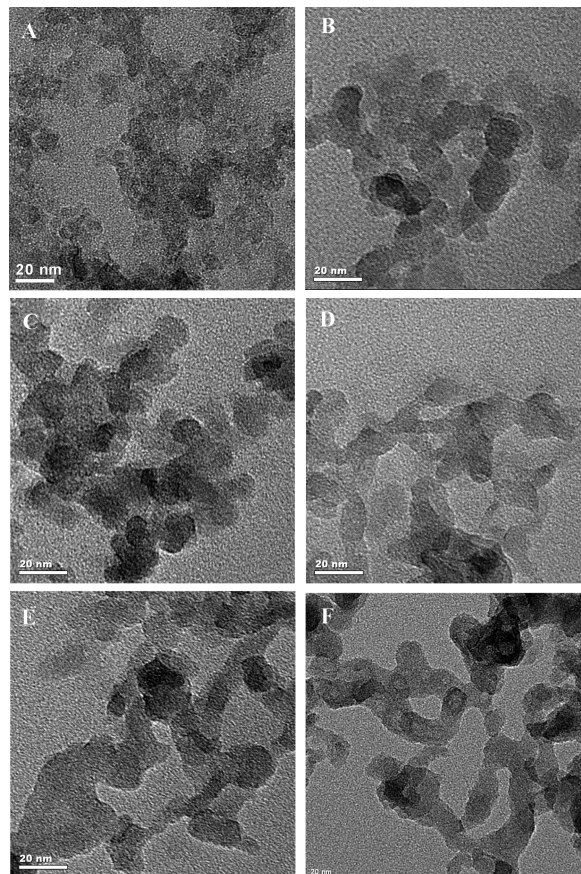


Figure 3. TEM images of the solid phases separated by LSC from the RM heated at 20 (A), 35 (B), 50 (C), 65 (D), 80 (E), and 170 °C (F) for $T_H = 1$ h. The scale bars represent 20 nm.

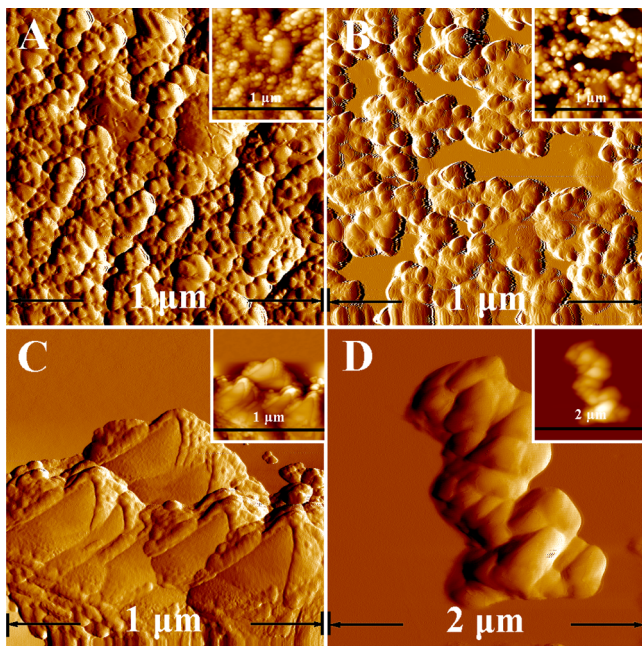
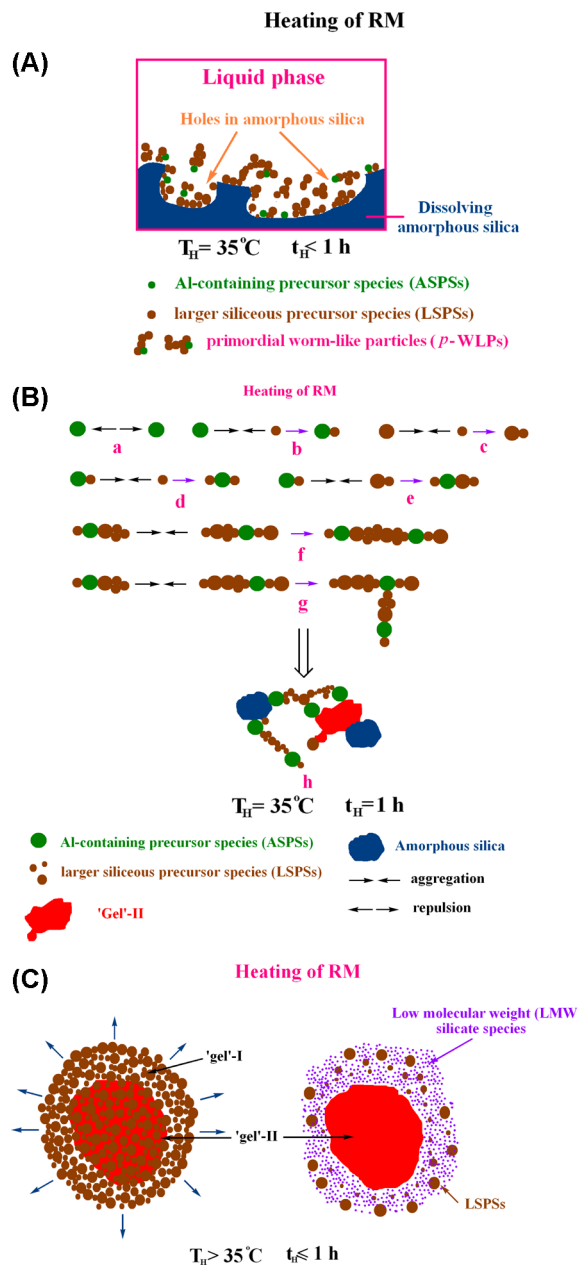


Figure 4. AFM images of the solid phases separated by LSC from the RM heated at 35 (A), 50 (B), 65 (C), and 80 °C (D) for $T_H = 1$ h. Panels A–D are presented in amplitude mode, and the insets are presented in height mode.

in the Supporting Information) and the changes of the concentrations of Si and Al in the liquid phase of RM. (See SI-1 in the Supporting Information.) These changes are the most intense just at the beginning of the heating of the RM from room temperature to 35 °C. Further dissolution of amorphous silica (see SI-1 in the Supporting Information) produces LMW silicate species, which participate in the further formation of the ~3 to ~15 nm sized precursor species (LSPSs), followed by formation of a new morphological feature, WLPs (compare the TEM images 3A and 3B and the AFM images 2A and 4A; see also Figures S6–S13 in the Supporting Information).

Thus, taking into consideration (i) the fact that the formation of WLPs was not observed in the early stage of crystallization of silicalite-1 (absence of Al)^{23,46} and (ii) the assumption that the formation of the WLPs starts after the “free” (discrete) Al-containing precursor species (ASPSs) are released from the Al-enriched amorphous silica during progressed dissolution at higher temperature(s), that is, $T_H >$ room temperature (Scheme 2A), the formation of the WLPs can be assumed as follows: Because of the repulsive forces, associated with the negative charges of the ($\equiv\text{Si}=\text{O}-\text{Al}\equiv$) links⁴² of the released ASPSs, these species cannot aggregate themselves but only with LSPSs (Scheme 2B). In this way, the LSPSs are “connective elements” between the ASPSs, that is, $-\text{ASPS}-(\text{LSPS})_n-\text{ASPS}-$, where the subscript n denotes the number of LSPSs in the array. Now, because (i) the rate of aggregation between ASPSs and LSPSs is generally higher than the rate of aggregation between LSPSs themselves,³⁷ (ii) ASPSs and LSPSs of different sizes are included in the aggregation/coalescence processes, and (iii) the rate of aggregation and the rate of coalescence of the collided/joined particles depend on their sizes,^{38–41} differently assembled “chains” of ASPSs and LSPSs (WLPs in the early stage of formation) can be formed by their aggregations, as shown in Figures 3B and 4A. (See also

Scheme 2. Schematic Presentation of the Processes Occurring During Heating of RMs



Scheme 2B.) Hence, the presence of Al is crucial for the formation of WLPs.²⁴ The role of Al is connected to the formation of “free” Al-containing precursor species (ASPSs); these species are formed during progressed dissolution of silica at higher temperature(s), that is, when the amorphous silica around the “protected area” has been completely dissolved (Scheme 2A). In addition, interactions of the formed “chains” result in the formation of a “network”, as is shown in Figure 3B and Figure S3.7 in the Supporting Information. (See also Scheme 2B,h.)

On the basis of the observed morphological changes of solid phase with increasing temperature (Figures 3 and 4), it is evident that evolution of early formed WLPs is temperature-dependent. This evolution is manifested by growth of the early formed WLPs, caused by the addition of the precursor species and followed by join together of the growing WLPs and gradual

coalescence of the discrete precursor species (Figures 3 and 4). At the heating temperature $T_H \geq 80^\circ\text{C}$, the discrete precursor species can be seldom recognized in the well-formed WLPs (Figure 3E,F).

On the other hand, Figures 3 and 4 also show that the “amounts” of both “gel”-I and “gel”-II decrease with the increase in the heating temperature, T_H , and that these features completely disappear at $T_H \geq 65^\circ\text{C}$. This shows that the increase in the temperature, T_H , causes disaggregation of “gel”-I and dissolution/disaggregation of “gel”-II (Scheme 2C). Disaggregation of “gel”-I produces discrete precursor species of different sizes (LSPSs). The dissolution of both “gel”-II and undissolved amorphous silica, respectively, produces LMW silicate species, which then aggregate into PPSs and further into precursor species (LSPSs, ASPSs) of different sizes (Schemes 1F,G and 2A). The precursor species produced by the described ways immediately participate not only in the formation of new WLPs but also in the growth of the already formed ones. In this way, the formation of the WLPs and their growth are dynamical processes, which take place simultaneously during the heating of RM.

Here it is interesting that the particle size distribution (PSD) of the solid phase does not considerably change in the temperature range from 20°C (Figure 1A,B) to 80°C (Figure 5B,B'). This indicates that all described processes take place

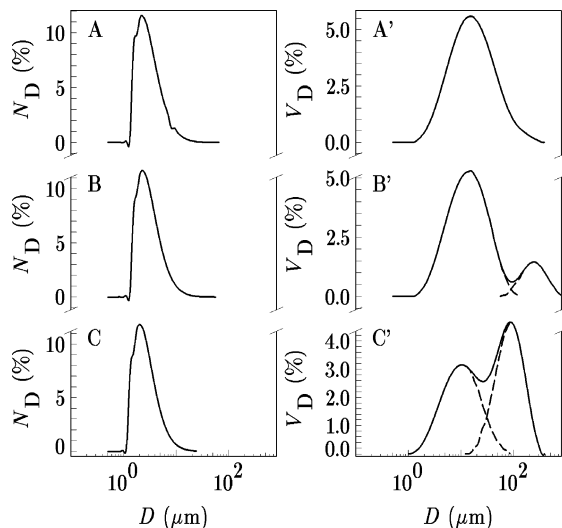


Figure 5. PSDs by number (A–C) and by volume (A'–C') of the solid phases of the reaction mixtures heated at 65 (A,A'), 80 (B,B'), and 170 °C (C,C') for $T_H = 1$ h. N_D is number percentage and V_D is volume (mass) percentage of the particles having the spherical equivalent diameter D .

“inside” the aggregates of the about 10 nm sized particles formed during the preparation of RM and its short time ($t_A = 1$ h) *rt* aging (Figure 1). More intense change of the PSD of the solid phase in the temperature range from $T_H = 80$ (Figure 5B') to 170 °C (Figure 5C') is explained in S2 of the Supporting Information.

The size of the particles, remaining in the liquid phase after the LSC of the RMs, does not considerably change from $T_H = 35$ to 50 °C but gradually decreases from $T_H = 50$ to 170 °C (Figure 6 and Table S3 in the Supporting Information). More interestingly, the PSDs of the particles remaining in the liquid phase after LSC of the RMs heated to 35 and 50 °C (○, dashed curves in Figures 6A',B') are almost the same as the PSD of the

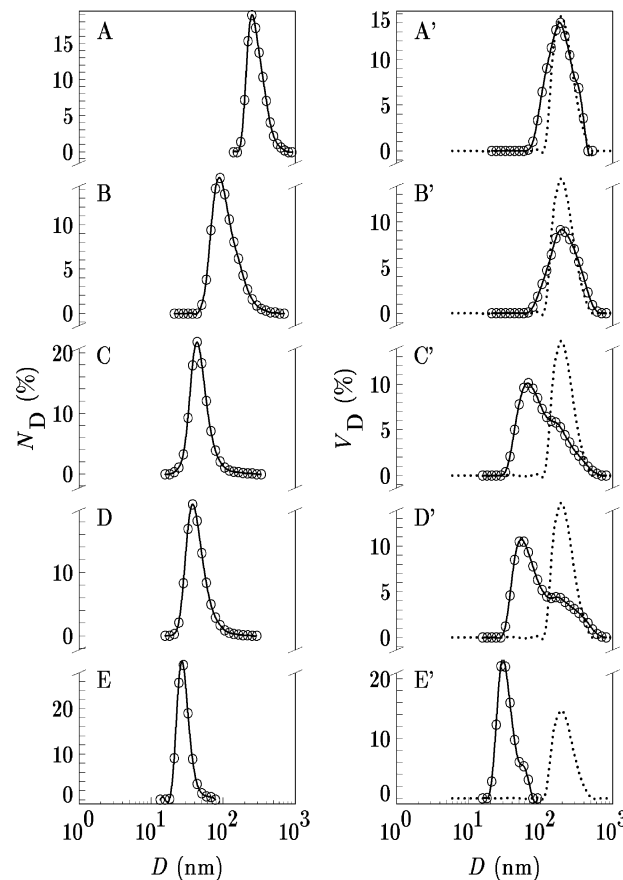


Figure 6. DLS-PSDs by number (A–E) and by volume (A'–E') of the liquid phases separated from the RMs heated at 35 (A,A'), 50 (B,B'), 65 (C,C'), 80 (D,D'), and 170 °C (E,E') for 1 h by LSC (○, dashed curves). The dotted curves represent the PSDs of the fumed silica. N_D is number percentage and V_D is volume (mass) percentage of the particles having the spherical equivalent diameter D .

fumed silica used as silica source (dotted curves in Figures 3A'–E'). This indicates that the dissolution of amorphous silica is accompanied not only by depletion of the aggregates ($D \approx 40$ –500 μm; Figure 1B), formed during short-time room-temperature aging of the RM, but also by the appearance of the particles of amorphous silica in the liquid phase of the RM (Figure 6). However, a gradual decrease in the size of the particles remained in the liquid phase after LSC for $T_H \geq 65^\circ\text{C}$ (Figure 6 and Table S3 in the Supporting Information) indicates that the particles of amorphous silica, dispersed in the liquid phase of RM, start to dissolve at $T_H \geq 65^\circ\text{C}$ or that a new population of smaller particles (see Table S3 in the Supporting Information) is formed at $T_H = 170^\circ\text{C}$.

Comparison of the TEM images relevant for the evolution of the particles dispersed in the liquid phase (Figure 7) with the TEM images relevant for the evolution of the solid phase (Figure 3) during heating of RMs shows that the processes occurring in the solid and in the liquid phase are almost the same, that is, the formation of LMW silicate species by dissolution of amorphous silica, their aggregation into PPSs and further into LSPSs, and finally, the formation and growth of the WLPs by aggregation of the LSPSs and ASPSs of different sizes. However, because of the considerably lower concentration of the LMW silicate species in the liquid phase than on the surfaces of the dissolving particles of amorphous silica (solid phase), the mentioned processes are faster in the solid than in

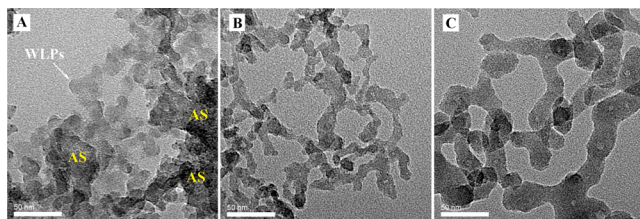


Figure 7. TEM images of the solid phase, separated by LSC/HSC from the RMs heated at 50 (A), 80 (B), and 170 °C (C) for 1 h. AS = amorphous silica, WLPs = worm-like particles. The scale bars represent 50 nm..

the liquid phase of RM, and the size (~ 30 nm; Figure 6E' and Table S3 in the Supporting Information) of the WLPs formed in the liquid phase is smaller than the size (~ 200 nm; Figure S13 in the Supporting Information) of the WLPs formed in the solid phase.²⁴

The “initial stage” of crystallization ends with the formation of the individual WLPs at $T_H = t_c = 4$ h (Figure S13 in the Supporting Information), as reported in our previous work.²⁴ In the following stages of crystallization, the as-formed WLPs gradually aggregate into rickety held aggregates at $T_H = t_c \approx 20$ h, which then, in <1 h, transform into CAs and further into polycrystalline aggregates of very small, nanosized ZSM-5 crystals. (See SI-3 in the Supporting Information.)

4. CONCLUSIONS

By careful analysis of the changes of chemical and morphological properties of the solid and the liquid phases of the model heterogeneous crystallization system, $12.5\text{Na}_2\text{O}-\text{Al}_2\text{O}_3-8\text{TPABr}-60\text{SiO}_2-4000\text{H}_2\text{O}$, during its short time (1 h) aging/heating at different temperatures (from 20 to 170 °C) using a series of characterization methods, it was found that these changes take place by a chain of events (Schemes 1 and 2):

(i) Incorporation of aluminate ions from solution onto the surfaces of the amorphous silica, used as silica source, thus forming the Al-enriched amorphous silica. This process starts at room temperature (*rt*) and continues during the heating of the RM.

(ii) Dissolution of the Al-enriched amorphous silica. Because of inertness of the surface Si–O–Al bonds on hydroxide attack, the dissolution of the Al-enriched silica results in the formation of LMW silicate species during both the *rt*-aging and heating of the RM. The concentration of the LMW silicate species is, at any temperature, largest at the places of formation (surfaces of the particles of amorphous silica) and decrease toward the bulk of the liquid phase).

(iii) Formation of the ~ 3 nm-sized core(amorphous silica)-shell($\text{Na}^+, \text{TPA}^+$) PPSs by a rapid aggregation of the LMW silicate species. By the reason explained in (ii), the “concentration” of the PPSs is, at any temperature, largest at the surfaces of the particles of amorphous silica and decreases toward the bulk of the liquid phase.

(iv) Formation of LSPSSs (~ 3 nm to ~ 15 nm sized) by aggregation of PPSs. Again, the “concentration” of the PPSs is, at any temperature, largest at the surfaces of the particles of amorphous silica and decreases toward the bulk of the liquid phase.

(v) Aggregation of the LSPSSs at the *rt* results in the formation of the randomly assembled aggregates (“gel”-primary amorphous precursor).

(vi) Early-stage formation of WLPs by aggregation of the LSPSSs and the Al-containing precursor species (ASPs), released from the Al-enriched amorphous silica during progressed dissolution at higher temperature(s) ($T_H \geq 35$ °C).

(vii) Growth of the early-stage formed WLPs by the addition of the LSPSSs formed by further (continuous) dissolution of the amorphous silica or by disaggregation/dissolution of “gel” ($T_H \geq 35$ °C).

(viii) “Ripening” of the WLPs by coalescence of the participating precursor species; this results in the formation of the “ripe” WLPs joined together with other WLPs and parts of undissolved amorphous silica ($T_H \geq 80$ °C).

The processes i–vii occur in both the solid and the liquid phase of RM; however, because of lower concentrations of the subcolloidal precursor species in the liquid phase, these processes are slower in the liquid phase than in the solid phase. In addition, in difference to ~ 200 nm sized WLPs (secondary amorphous precursor) formed in the solid phase and then aggregated into CAs (tertiary amorphous precursor) during the prolonged heating of RM, the WLPs formed in the liquid phase are considerably smaller (~ 30 nm) and do not aggregate during the prolonged heating of RM.

Similar methodology will be applied in the further studies on the early stage of crystallization of different types of zeolites in heterogeneous systems, under different conditions, to find a possible relationship between the described features/events and the crystallization of different types of zeolites.

ASSOCIATED CONTENT

S Supporting Information

Changes of concentrations of Si and Al in the liquid phase (SI-1). Additional particle size distribution data (SI-2). Detailed analyses of FE-SEM, TEM, and AFM images (SI-3). This material is available free of charge via the Internet at <http://pubs.acs.org>.

AUTHOR INFORMATION

Corresponding Authors

*N.R.: E-mail: nanren@fudan.edu.cn.

*B.S.: E-mail: subotic@irb.hr.

Notes

The authors declare no competing financial interest.

ACKNOWLEDGMENTS

This work is supported by “Chen Guang” project supported by Shanghai Municipal Education Commission and Shanghai Education Development Foundation (09CG02), project 098-0982904-2953, financially supported by the Ministry of Science, Education and Sport of the Republic of Croatia, and “China-Croatia” bilateral project supported by both the Ministry of Science and Technology of People’s Republic of China and the Ministry of Science, Education and Sport of the Republic of Croatia (2014-2015).

REFERENCES

- Davis, M. E. Zeolites and molecular sieves - not just ordinary catalysts. *Ind. Eng. Chem. Res.* **1991**, *30*, 1675–1683.
- Subotić, B.; Bronić, J.; Antonić Jelić, T. Theoretical and Practical Aspects of Zeolite Nucleation. In *Ordered Porous Solids*; Valtchev, V., Mintova, S., Tsapatsis, M., Eds.; Elsevier: Amsterdam, 2008; Ch. 6, pp 127–185.

- (3) Cundy, C. S.; Cox, P. A. The hydrothermal synthesis of zeolites: Precursors, intermediates and reaction mechanism. *Microporous Mesoporous Mater.* **2005**, *82*, 1–78.
- (4) Schoeman, B. J. A high temperature in situ laser light-scattering study of the initial stage in the crystallization of TPA-silicalite-1. *Zeolites* **1997**, *18*, 97–105.
- (5) de Moor, P.-P. E. A.; Beelen, T. P. M.; van Santen, R.; Beck, L. W.; Davis, M. E. Si-MFI crystallization using a “dimer” and “trimer” of TPA studied with small-angle X-ray scattering. *J. Phys. Chem. B* **2000**, *104*, 7600–7611.
- (6) Kirschhock, C. E. A.; Buschmann, V.; Kremer, S.; Ravishankar, R.; Houssin, C. J. Y.; Mojet, B. L.; van Santen, R. A.; Grobet, P. J.; Jacobs, P. A.; Martens, J. A. Zeosil nanoslabs: Building blocks in nPr(4)N(+)-mediated synthesis of MFI zeolite. *Angew. Chem., Int. Ed.* **2001**, *40*, 2367–2640.
- (7) Fedeyko, J. M.; Rimer, J. D.; Lobo, R. F.; Vlachos, D. G. Spontaneous formation of silica nanoparticles in basic solutions of small tetraalkylammonium cations. *J. Phys. Chem. B* **2004**, *108*, 12271–12275.
- (8) Provis, J. L.; Vlachos, D. G. Silica nanoparticle formation in the TPAOH-TEOS-H₂O system: A population balance model. *J. Phys. Chem. B* **2006**, *110*, 3098–3108.
- (9) Nikolakis, V.; Kokkoli, E.; Tirrell, M.; Tsapatsis, M.; Vlachos, D. G. Zeolite growth by addition of subcolloidal particles: Modeling and experimental validation. *Chem. Mater.* **2000**, *12*, 845–853.
- (10) Mintova, S.; Olson, N.H.; Senker, J.; Bein, T. Mechanism of the transformation of silica precursor solutions into Si-MFI zeolite. *Angew. Chem., Int. Ed.* **2002**, *41*, 2558–2561.
- (11) Hsu, C.-Y.; Chiang, A. S. T.; Selvin, R.; Thompson, R. W. Rapid synthesis of MFI zeolite nanocrystals. *J. Phys. Chem. B* **2005**, *109*, 18804–18814.
- (12) Aerts, A.; Haouas, M.; Caremans, T. P.; Follens, L. R. A.; van Erp, T. S.; Taulelle, F.; Vermant, J.; Martens, J. A.; Kirschhock, C. E. A. Investigation of the Mechanism of Colloidal Silicalite-1 Crystallization by Using DLS, SAXS, and Si-29 NMR Spectroscopy. *Chem.—Eur. J.* **2010**, *16*, 2764–2774.
- (13) Knight, C. T. G.; Wang, J. P.; Kinrade, S. D. Do zeolite precursor species really exist in aqueous synthesis media? *Phys. Chem. Chem. Phys.* **2006**, *8*, 3099–3103.
- (14) Fyfe, C. A.; Darton, R. J.; Schneider, C.; Scheffler, F. Solid-state NMR investigation of the possible existence of “Nanoblocks” in the clear solution synthesis of MFI materials. *J. Phys. Chem. C* **2008**, *112*, 80–88.
- (15) Davis, T. M.; Drews, T. O.; Ramanan, H.; He, C.; Dong, J.; Schnablegger, H.; Katsoulakis, M. A.; Kokkoli, E.; McCormick, A. V.; Lee Penn, R.; Tsapatsis, M. Mechanistic principles of nanoparticle evolution to zeolite crystals. *Nat. Mater.* **2006**, *5*, 400–408.
- (16) Aerts, A.; Kirschhock, C. E. A.; Martens, J. A. Methods for in situ spectroscopic probing of the synthesis of a zeolite. *Chem. Soc. Rev.* **2010**, *39*, 4626–4642.
- (17) Hould, N. D.; Haouas, M.; Nikolakis, V.; Taulelle, F.; Lobo, R. F. Mechanisms of Quick Zeolite Beta Crystallization. *Chem. Mater.* **2012**, *24*, 3621–3632.
- (18) Hould, N. D.; Kumar, S.; Tsapatsis, M.; Nikolakis, V.; Lobo, R. F. Structure and Colloidal Stability of Nanosized Zeolite Beta Precursors. *Langmuir* **2010**, *26*, 1260–1270.
- (19) Padovan, M.; Leofanti, G.; Solari, M.; Moretti, E. Studies on the ZSM-5 zeolite formation. *Zeolites* **1984**, *4*, 295–299.
- (20) Scholle, K. F. M. G. J.; Veeman, W. S.; Frenken, P.; van der Velden, G. P. M. Characterization of intermediate TPA-ZSM-5 type structures during crystallization. *Appl. Catal.* **1985**, *17*, 233–259.
- (21) Salou, M.; Kooli, F.; Kiyozumi, Y.; Mikamizu, F. Effect of aluminium source and content on the synthesis of zeolite ZSM-5 from kanemite via solid-state transformation. *J. Mater. Chem.* **2001**, *11*, 1476–1481.
- (22) Burkett, S. L.; Davis, M. E. Mechanisms of structure direction in the synthesis of pure-silica zeolites. 1. Synthesis of TPA/Si-ZSM-5. *Chem. Mater.* **1995**, *7*, 920–928.
- (23) Kosanović, C.; Havensack, K.; Subotić, B.; Svetličić, V.; Mišić, T.; Cziraki, A.; Huhn, G. A contribution to understanding the mechanism of crystallization of silicalite-1 in heterogeneous systems (hydrogels). *Microporous Mesoporous Mater.* **2009**, *123*, 150–159.
- (24) Ren, N.; Subotić, B.; Bronić, J.; Tang, Y.; Dutour Sikirić, M.; Mišić Radić, T.; Svetličić, V.; Bosnar, S.; Antonić Jelić, T. Unusual pathway of crystallization of zeolite ZSM-5 in a heterogeneous system: phenomenology and starting considerations. *Chem. Mater.* **2012**, *24*, 1726–1737.
- (25) Ren, N.; Bronić, J.; Bosnar, S.; Dutour Sikirić, M.; Antonić Jelić, T.; Mao, J.-J.; Subotić, B. The relationship between sub-micrometer sized ZSM-5, slice-like (lamellar) keatite and hollow alpha-quartz particles: a phase transformation study. *CrystEngComm.* **2013**, *15*, S032–S044.
- (26) Iller, R. K. *The Chemistry of Silica*; John Wiley: New York, 1979.
- (27) Harvey, G.; Dent Glasser, L. S. Structure and properties of aluminosilicate solutions and gels. *ACS Symp. Ser.* **1989**, *398*, 49–65.
- (28) Lindner, T.; Lechert, H. The influence of fluoride on the crystallization of zeolite NaY. *Zeolites* **1994**, *14*, 582–587.
- (29) Gabelica, Z.; Derouane, E. G.; Blom, N. Factors affecting the synthesis of pentasil zeolites. *Acs. Symp. Ser.* **1984**, *248*, 219–251.
- (30) Barrer, R. M. *Hydrothermal Chemistry of Zeolites*; Academic Press: London, 1982.
- (31) Engelhardt, G.; Fahlke, B.; Mägi, M.; Lippmaa, E. High-resolution solid-state Si-29 and Al-27 NMR of aluminosilicate intermediates in the synthesis of zeolite-A. Part II. *Zeolites* **1985**, *5*, 49–52.
- (32) Szostak, R. *Molecular Sieves: Principles of Synthesis and Identification*; Van Nostrand Reinhold: New York, 1989.
- (33) Swaddle, T. W. Silicate complexes of aluminum(III) in aqueous systems. *Coord. Chem. Rev.* **2001**, *219*, 665–686.
- (34) Kinrade, S. D.; Knight, C. T. G.; Pole, D. L.; Svytski, R. T. Silicon-29 NMR studies of tetraalkylammonium silicate solutions. 1. Equilibria, Si-29 chemical shifts, and Si-29 relaxation. *Inorg. Chem.* **1998**, *37*, 4272–4277.
- (35) Kinrade, S. D.; Knight, C. T. G.; Pole, D. L.; Svytski, R. T. Silicon-29 NMR studies of tetraalkylammonium silicate solutions. 2. Polymerization kinetics. *Inorg. Chem.* **1998**, *37*, 4278–4283.
- (36) Rimer, J. D.; Lobo, R. F.; Vlachos, D. G. Physical basis for the formation and stability of silica nanoparticles in basic solutions of monovalent cations. *Langmuir* **2005**, *21*, 8960–8971.
- (37) Fedeyko, J. M.; Egolf-Fox, H.; Fickel, D. W.; Vlachos, D. G.; Lobo, R. F. Initial stages of self-organization of silica-alumina gels in zeolite synthesis. *Langmuir* **2007**, *23*, 4532–4540.
- (38) Friedlander, S. K.; Wu, M. K. Linear rate law for the decay of the excess surface-area of a coalescing solid particle. *Phys. Rev. B* **1994**, *49*, 3622–3624.
- (39) Lehtnen, K. E. J.; Windeler, R. S.; Friedlander, S. K. A note on the growth of primary particles in agglomerate structures by coalescence. *J. Colloid Interface Sci.* **1996**, *182*, 606–608.
- (40) Hawa, T.; Zachariah, M. R. Coalescence kinetics of unequal sized nanoparticles. *J. Aerosol Sci.* **2006**, *37*, 1–15.
- (41) Wang, J. M.; Lin, J. Z. Collision efficiency of two nanoparticles with different diameters in Brownian coagulation. *J. Appl. Math. Mech. (Engl. Transl.)* **2011**, *32*, 1019–1028.
- (42) Čižmek, A.; Subotić, B.; Aiello, R.; Crea, F.; Nastro, A.; Tuoto, C. Dissolution of high-silica zeolites in alkaline-solutions. 1. Dissolution of silicalite-1 and ZSM-5 with different aluminum content. *Microporous Mater.* **1995**, *4*, 159–168.
- (43) Groen, J. C.; Peffer, L. A. A.; Moulijn, J. A.; Perez-Ramirez, J. On the introduction of intracrystalline mesoporosity in zeolites upon desilication in alkaline medium. *Microporous Mesoporous Mater.* **2004**, *69*, 29–34.
- (44) Groen, J. C.; Peffer, L. A. A.; Moulijn, J. A.; Perez-Ramirez, J. Mechanism of hierarchical porosity development in MFI zeolites by desilication. The role of aluminium as a pore-directing agent. *Chem.—Eur. J.* **2005**, *11*, 4983–4994.

(45) Na, K.; Choi, M.; Ryoo, R. Recent advances in the synthesis of hierarchically nanoporous zeolites. *Microporous Mesoporous Mater.* **2013**, *166*, 3–19.

(46) Lupulescu, A. I.; Rimer, J. D. In situ imaging of silicalite-1 surface growth reveals the mechanism of crystallization. *Science* **2014**, *344*, 729–732.